doi:10.1016/j.jmb.2007.08.056 J. Mol. Biol. (2007) 373, 1229–1242

JMB

Available online at www.sciencedirect.com

ScienceDirect

ELSEVIER

Structural Insights into the Conformational Variability of FtsZ

María A. Oliva, Daniel Trambaiolo and Jan Löwe*

MRC Laboratory of Molecular Biology Hills Road, Cambridge CB2 2QH, UK

Received 18 July 2007; received in revised form 22 August 2007; accepted 23 August 2007
Available online 29 August 2007

FtsZ is a prokaryotic homologue of the eukaryotic cytoskeletal protein tubulin and plays a central role in prokaryotic cell division. Both FtsZ and tubulin are known to pass through cycles of polymerization and depolymerization, but the structural mechanisms underlying this cycle remain to be determined. Comparison of tubulin structures obtained in different states has led to a model in which the tubulin monomer undergoes a conformational switch between a "straight" form found in the walls of microtubules and a "curved" form associated with depolymerization, and it was proposed recently that this model may apply also to FtsZ. Here, we present new structures of FtsZ from47 *Aquifex aeolicus*,47 *Bacillus subtilis*, *Methanococcus jannaschii* and *Pseudomonas aeruginosa* that provide strong constraints on any proposed role for a conformational switch in the FtsZ monomer. By comparing the full range of FtsZ structures determined in different crystal forms and nucleotide states, and in the presence or in the absence of regulatory proteins, we find no evidence of a conformational change involving domain movement. Our new structural data make it clear that the previously proposed straight and curved conformations of FtsZ were related to inter-species differences in domain orientation rather than two interconvertible conformations. We propose a new model in which lateral interactions help determine the curvature of protofilaments.

Edited by M. Moody

Keywords: FtsZ; tubulin; bacterial cell division; crystal structure; divisome

Introduction

FtsZ, a highly conserved cytoskeletal protein involved in bacterial cell division, is the first protein known to localize to the division site, where it polymerizes to form a dynamic ring structure known as the Z ring.[1,2] The polymerization dynamics of FtsZ depend on its properties as a GTPase: nucleotide binding promotes longitudinal association of monomers into protofilaments, while hydrolysis leads to protofilament disassembly.[3–5] Despite extensive investigations into FtsZ behaviour both *in vivo* and *in vitro*, its precise role and mechanism in cell division remain unclear.[6–9] Recent evidence suggests that, in addition to its role in septum formation, FtsZ may have a role in cell wall elongation.[10–12]

The monomer and protofilament structures of FtsZ are similar to those of its eukaryotic homologue tubulin,[13–15] and improved understanding of the mechanisms of each of these proteins may yield insights that are relevant to the other. Tubulin αβ-heterodimers assemble into microtubules, which are long hollow cylinders composed of laterally associated straight protofilaments. The GTPase activity of β-tubulin is activated in the polymer, and the dynamic instability of microtubules arises from the fact that the thermodynamically unstable GDP-bound protofilaments are held in a metastable polymerized state by lateral interactions and the presence of a GTP-bound cap. Loss of the GTP cap leads to rapid depolymerization of the microtubule. Dynamic instability requires that GDP in the polymer cannot exchange with GTP. The mechanics of depolymerization are thought to play a role in generating the force for sister chromatid separation during mitosis.[16–18]

FtsZ monomers form protofilaments that are similar to those of tubulin; although lateral association of FtsZ protofilaments has been observed *in vitro*, the molecular details and physiological relevance of this bundling are unclear.[19,20] FtsZ protofilaments can

*Corresponding author. E-mail address: jyl@mrc-lmb.cam.ac.uk.

be straight or curved, and other morphologies including sheets, tubes, minirings and helices have been observed *in vitro*, depending on the experimental conditions used.[21,22] In contrast to tubulin, FtsZ filaments are thought not to display dynamic instability, and biochemical experiments suggest that FtsZ polymers undergo rapid exchange of either nucleotide or monomers, either of which would be incompatible with dynamic instability.[23,24] It is not known whether the Z ring has a direct mechanical role in cell division or merely serves as a scaffold for the recruitment of other cell division proteins.

FtsZ and tubulin share a distinctive fold with a two-domain architecture: an N-terminal nucleotide-binding domain is connected *via* a central helix (H7) to a C-terminal domain that is involved in forming the protofilament.[13,14] The GTPase active site is formed at the interface between monomers by insertion of acidic residues from the C-terminal domain's T7 (synergy) loop into the nucleotide-binding pocket of the preceding monomer in the protofilament. In the case of FtsZ, the unit of polymerization is the monomer, while in the case of tubulin it is the αβ-tubulin heterodimer. α-Tubulin and β-tubulin each bind one nucleotide molecule. α-Tubulin remains GTP-bound and associated stably with β-tubulin because the T7 loop of β-tubulin lacks the acidic residue that would be needed to complete the α-tubulin active site.[14]

Structures of tubulin in different states reveal the existence of distinct conformations of the tubulin monomer: a "straight" conformation found in the straight protofilaments of microtubules and flat Zn-induced sheets,[14,25] and a "curved" conformation seen in co-crystals of αβ-tubulin with colchicine and the RB3 stathmin-like domain,[26] and in helical ribbons.[27] γ-Tubulin[28] and BtubA/B[29] have a conformation similar to the curved conformation of αβ-tubulin. The conformational switch involves a change in the packing angle between the tubulin N-terminal and C-terminal domains (8° in α-tubulin and 11° in β-tubulin) coupled with a shift in the position of the central helix H7 (1.5 Å in α-tubulin and 2.5 Å in β-tubulin). Somewhat surprisingly, both the α and β-tubulin subunits of the tubulin heterodimer seem to undergo this switch in a concerted fashion, despite the fact that only β-tubulin alters its nucleotide state. This observation suggests that the tubulin conformational switch, unlike the classical conformational switches seen in small GTPases,[30–33] is dependent on the longitudinal and lateral interactions between monomers rather than on nucleotide content alone. It has been proposed that the conformational switch plays a role in force generation by depolymerizing microtubules, perhaps acting as a power stroke as the protofilament curls outwards from the microtubule wall.[34,35]

Does FtsZ undergo a conformational switch similar to that proposed for tubulin? We have determined the structure of *Methanococcus jannaschii* FtsZ (MjFtsZ) in different nucleotide states and found no evidence of significant conformational changes, despite the fact that the crystal packing in one crystal form creates interfaces between monomers similar to those found in the protofilament.[36] However, a recent comprehensive analysis of all available FtsZ structures found that the conformation of *Pseudomonas aeruginosa* FtsZ (PaFtsZ) bound to the inhibitory protein SulA differed from the conformations of free FtsZ protein from other species in a manner that resembled the tubulin straight–curved conformational switch.[37]

Here, we present the structures of FtsZ from *Bacillus subtilis* (BsFtsZ) and *Aquifex aeolicus* (AaFtsZ), as well as the structure of free FtsZ from *P. aeruginosa* and a new high-resolution structure of *Methanococcus jannaschii* FtsZ (MjFtsZ), and analyse the implications of these new structures for our understanding of FtsZ conformational mechanics. The structure of *B. subtilis* FtsZ shows no unusual feature, but we find that crystals of *A. aeolicus* FtsZ contain an alternative mode of packing at the protofilament interface, suggesting the degree of flexibility that this interface might be able to accommodate. Comparison of the structures of SulA-bound and free *P. aeruginosa* FtsZ reveals no significant conformational change, and we conclude that the differences between *P. aeruginosa* and *M. jannaschii* FtsZ are due simply to their different primary sequences rather than the presence of a conformational switch that depends on the nucleotide state of the monomeric protein. A comprehensive structural analysis of all available structures reveals the intrinsic variability of the relative positioning of FtsZ between the N-terminal and C-terminal domains in different species. Finally, we present a model for the FtsZ polymerization cycle, taking into account the lack of a nucleotide-dependent conformational change in the monomer.

Results and Discussion

Structure of FtsZ from *B. subtilis*

We have solved the structure of untagged, full-length *B. subtilis* FtsZ at a resolution of 2.5 Å (Figure 1(a)). Although the crystals grew only in the presence of FtsZ inhibitor dichamanetin,[38] we were unable to locate the inhibitor in the final electron density maps. The overall structure of BsFtsZ is similar to previously solved FtsZ structures. No electron density was visible for the N-terminal residues 1–12 or the C-terminal residues 316–382. The structure shows BsFtsZ in its empty form: nucleotide content analysis of the protein used for crystallization yielded a GXP: FtsZ ratio of 0.07, and the crystallographic electron density maps show that the nucleotide-binding pocket is empty apart from a bound sulfate ion. It is worth highlighting that the nucleotide-binding pocket is blocked by helix H2 and loop T3 of the next molecule in the crystal lattice, which precludes dichamanetin or nucleotide soaking experiments.

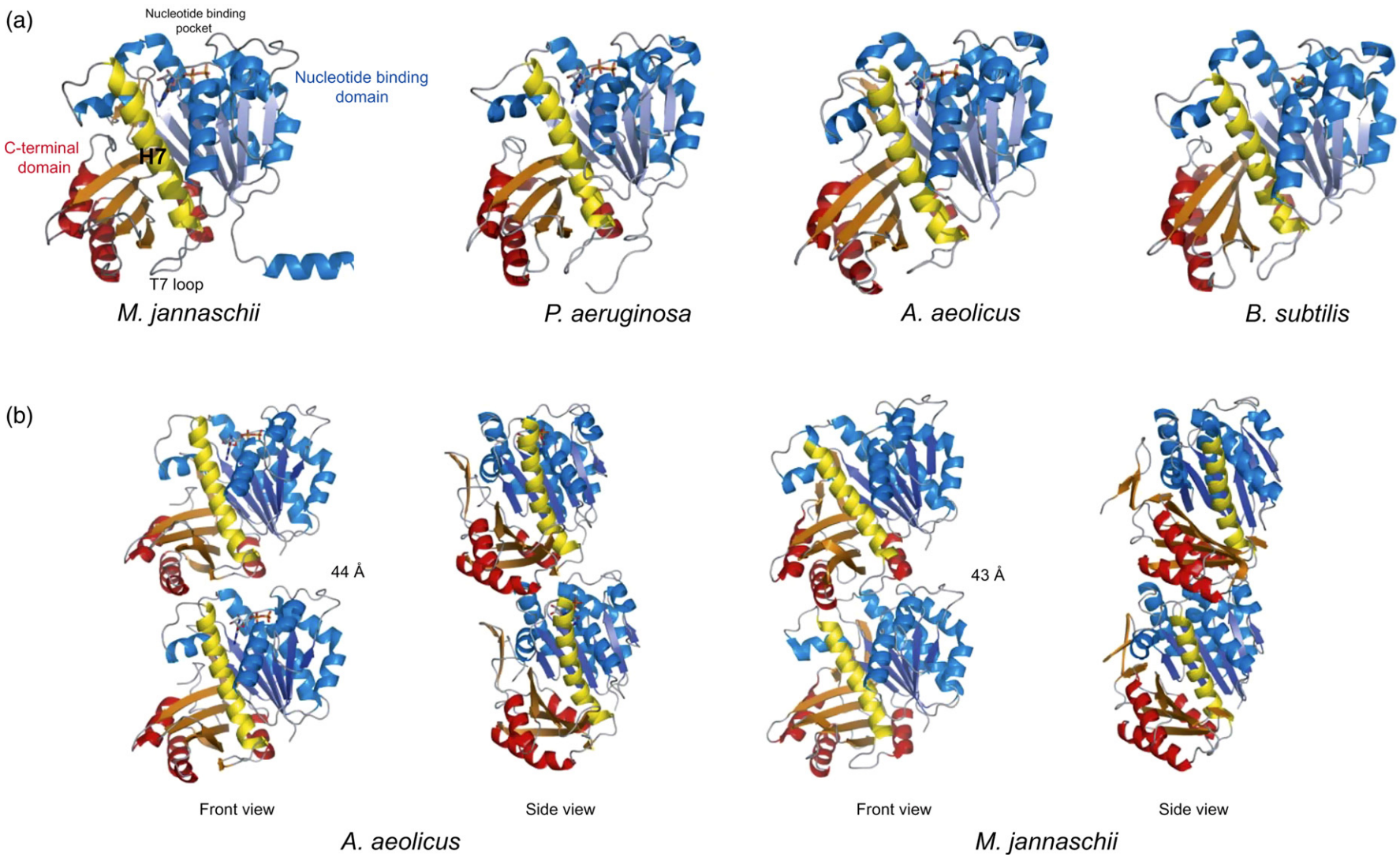

Figure 1. (a) Ribbon representation of FtsZ structures from *M. jannaschii*, *P. aeruginosa* (residues 2–316), *A. aeolicus* (residues 4–326) and *B. subtilis* (residues 12–315). The nucleotide-binding domain is coloured dark/light blue, the core helix H7 yellow, and the C-terminal domain red/orange. (b) Protofilament-like structures in crystals of GDP-bound *A. aeolicus* FtsZ (PDB ID 2RGR) and empty *M. jannaschii* FtsZ (PDB ID 1W59). The protofilament interface is altered by a sliding movement of the top subunit with respect to the lower subunit in the *Aquifex* structure (left) and is distorted by a rotation of about 10° in the *Methanococcus* structure (right).

Table 1. Summary of FtsZ structures used/solved in this study

	Methanococcus jannaschii						
PDB entry	2VAP	1FSZ	1W58	1W59	1W5B	1W5A	1W5E
Protein length	364 (C-terminal His-tag protein)	364 (C-terminal His-tag protein)	364 (C-terminal His-tag protein)	364 (C-terminal His-tag protein)	364 (C-terminal His-tag protein)	364 (C-terminal His-tag protein)	364 (mutation W319Y, no tag)
Purification method	Ni-NTA affinity chromatography under denaturing conditions, refolded and gel filtration	Ni-NTA affinity cromatography and gel filtration	Ni-NTA affinity cromatography and gel filtration	Ni-NTA affinity chromatography under denaturing conditions, refolded and gel filtration	Ni-NTA affinity chromatography under denaturing conditions, refolded and gel filtration	Ni-NTA affinity chromatography under denaturing conditions, refolded and gel filtration	HiTrap-Q anion exchange chromatography, HiTrap Phenyl Sepharose HP hydrophobic chromatography and gel filtration
Space group	$P3_121$	$I2_13$	$I2_13$	$P2_1$	$P2_1$	$P2_1$	$P1$
Resolution (Å)	1.7	2.8	2.5	2.7	2.2	2.4	3.0
Chains per asymmetric unit	1 (monomer)	1 (monomer)	1 (monomer)	2 (longitudinal dimer)	2 (longitudinal dimer)	2 (longitudinal dimer)	9 (monomer)
R	0.179	0.199	0.221	0.216	0.209	0.218	0.264
R_{free}	0.208	0.282	0.253	0.296	0.259	0.264	0.298
Nucleotide binding site	GDP	GDP	GMPCPP/Mg^{2+} (soak of 1FSZ)	No nucleotide but SO_4^- in both chains	GTP in both chains (soak of 1W59)	GTP/Mg^{2+} chain A GTP chain B (soak of 1W59)	GTP all the chains
Chain ordered in the unit cell	20–354	23–356	23–363	A 3–17, 20–354 B 22–364	A 22–355 B 22–357	A 22–355 B 22–357	23–354 chains A,C,D,F,G,I 23–355 chains B, E, H

	Pseudomonas aeruginosa		*Mycobacterium tuberculosis*			*Thermotoga maritima*	*Bacillus subtilis*	*Aquifex aeolicus*
PDB entry	1OFU	2VAW	1RQ2	1RQ7	1RLU	1W5F	2VAM	2RGR
Protein length	318 (full length protein 394, N-terminal Strep-tag and C-terminal His-tag)	318 (full length protein 394, N-terminal Strep-tag and C-terminal His-tag)	379 (N-terminal His-tag)	379 (N-terminal His-tag)	379 (N-terminal His-tag)	351 (T7 loop change from 217 to IRLTSRFARIE, C-terminal His-tag)	382 (no tag)	331 (full length 368, C-terminal His-tag
Purification method	Ni-NTA affinity chromatography and gel filtration	HiTrap Q anion exchange chromatography and gel filtration	Ni^{2+} affinity chromatography, thrombin His-tag remove and gel filatration	Ni^{2+} affinity chromatography, thrombin His-tag remove and gel filatration	Ni^{2+} affinity chromatography, thrombin His-tag remove and gel filatration	Ni-NTA affinity cromatography and gel filtration	HiTrap Q anion exchange chromatography and gel filtration	Ni-NTA affinity cromatography and gel filtration
Space group	$P2_12_12_1$	$P6_3$	$P6_5$	$P6_5$	$P6_5$	$P2_12_12$	$P3_221$	$P2_1$
Resolution (Å)	2.1	2.9	1.9	2.6	2.0	2.0	2.5	1.7
Chains per asymmetric unit	4 (central dimer of SulA and one FtsZ molecule bind to each SulA	1 (monomer)	2 (lateral dimer)	2 (lateral dimer)	2 (lateral dimer)	2 (domain-swapped dimer)	1 (monomer)	1 (monomer)
R	0.216	0.206	0.187	0.184	0.180	0.203	0.218	0.179
R_{free}	0.255	0.316	0.222	0.242	0.224	0.234	0.267	0.227
Nucelotide binding site	GDP	GDP	Citrate chain A Empty chain B	GDP chain A Empty chain B	GTP-γ-S chain A Empty chain B	GMPCPP/ Mg^{2+} both chains	No nucleotide but SO_4^-	GDP
Chain order in the unit cell	A 11–317 B 11.317	2–316	A 8–63, 69–312 B 8–59, 70–169, 174–313	A 8–63, 69–312 B 6–59, 70–170, 174–313	A 8–312 B 6–59, 70–169, 174–312	A 22–337 B 22–337	12–315	8–326

High-resolution structure of FtsZ from *M. jannaschii*

We have solved MjFtsZ in a new crystal form that yielded diffraction data to 1.7 Å resolution. The electron density maps revealed the presence of GDP in the nucleotide-binding pocket, without a magnesium ion. Helix H0 is in a different position when compared with PDB ID 1FSZ. After aligning the N-terminal domains, the key residues in the C-terminal domains (Table 2) show an rmsd of 1.2 Å. This difference between two structures in the same nucleotide state but in different crystal contexts gives an indication of the inherent flexibility of the FtsZ monomer.

Structure of FtsZ from *A. aeolicus*

FtsZ from *Aquifex aeolicus* was crystallized as a C-terminally truncated construct lacking residues 331–367, since full-length protein produced only poor-quality crystals and primary sequence analysis suggested that these residues were likely to be unstructured. The AaFtsZ crystals diffracted to a resolution of 1.7 Å (Figure 1(a)). The crystals contain one molecule of AaFtsZ per asymmetric unit, and electron density is clearly defined for residues 8–326 and bound GDP.

The packing of the AaFtsZ molecules in the crystal is somewhat similar to the arrangement thought to occur in the protofilament (Figure 1(b)). We suggested earlier that the best high-resolution model for the FtsZ protofilament is found in crystals of the GTP/Mg^{2+}-soaked form of MjFtsZ (PDB ID 1W5A): one dimer seen in these crystals is closely similar to the αβ-tubulin dimer, and the two aspartic acid residues in the T7 loop, which are known to form part of the protofilament's active site, are positioned to activate a water molecule for nucleophilic attack on the γ-phosphate group.[36] The new AaFtsZ crystals contain an interface between the monomers that is similar to the interface seen in the MjFtsZ dimer, although the contact area is less extensive. The repeat distance between AaFtsZ monomers is 44 Å, slightly longer than the 43 Å spacing seen in the crystallographic dimer of MjFtsZ and the 42–43 Å distance of EcFtsZ and MjFtsZ sheets measured by electron microscopy.[20,39] The adjacent monomers are positioned such that Asp206 and Asp209 of the synergy loop involved in catalysis are shifted away from the active site. Asp206 forms a salt-bridge with Lys139, whose positive charge is widely conserved in FtsZ from different species.

The differences between the pseudo-protofilament interfaces in MjFtsZ and AaFtsZ crystals may be related, in part, to the nucleotide state. It is possible to soak GTP into the MjFtsZ crystals and the structure that results appears to be poised in preparation for catalysis: the crystal packing was thus interpreted as representing the GTP-bound form of the protofilament. The AaFtsZ crystals were grown in the presence of GDP and contain GDP in the active site, and it was not possible to obtain a GTP-bound form by soaking. However, we have recently managed to obtain co-crystals of AaFtsZ with the inhibitor 8-morpholino-GTP, again at very high resolution (1.4 Å, in collaboration with Tanneke den Blaauwen, Amsterdam, unpublished results). Despite the additional presence of the nucleotide γ-phosphate group and a bound magnesium ion, these crystals are essentially identical with the GDP-bound crystals that we describe here. The lack of a conformational change in AaFtsZ induced by the presence of the γ-phosphate group reinforces the previously reported observation that monomeric FtsZ shows no structural change between its empty, GDP-bound and GTP-bound forms.[36]

The movement of the catalytic aspartic acid residues away from the active site is not entirely surprising if the crystal packing mimics the post-hydrolysis state of the protofilament. The docking interface between adjacent monomers in true protofilaments may permit greater flexibility than is commonly assumed. Similar flexibility in the protofilament interface can be seen by comparing the different αβ-tubulin structures determined by electron crystallography of Zn-induced sheets,[14,35] electron microscopic reconstruction of helical tubes formed in the presence of GDP or GMPPCP,[40] and X-ray crystallography of αβ-tubulin in complex with the RB3 stathmin-like domain and colchicines.[26] These changes in docking between tubulin monomers contribute substantially to the curvature of tubulin protofilaments in their curved state, in addition to some flexibility within the subunits, and it is likely that the same is true of FtsZ.

Structure of SulA-free FtsZ from *P. aeruginosa*

PaFtsZ was crystallized in the absence of SulA using the previously described C-terminally truncated construct lacking 76 residues.[41] Crystals containing a single molecule per asymmetric unit diffracted to a resolution of 2.9 Å, and the structure was solved by molecular replacement (Figure 1(a)). Nucleotide content of the purified protein showed a GXP/FtsZ ratio of 0.35 after gel filtration, and electron density maps indicated the presence of GDP in the nucleotide-binding pocket. Magnesium was not present in the crystallization conditions, and no magnesium ion was visible in the electron density maps.

Superposition of FtsZ structures and determination of domain angles

We aligned all previously available and new FtsZ structures (Table 1) using 56 residues from the core secondary structural elements of the highly conserved N-terminal domain (Table 2). The domain-swapped dimer of *Thermotoga maritima* FtsZ (TmFtsZ) and one chain of *Mycobacterium tuberculosis* FtsZ (MtFtsZ) were excluded from the analysis, since these structures contain distortions due to the changes in loop T7 (TmFtsZ) or crystal contacts (MtFtsZ) that are unlikely to be physiologically

Table 2. Residues selected for aligning the nucleotide-binding domains (top) and for the determination of rmsd values and angles between C-terminal domains (bottom)

Nucleotide-binding domain fitting						
Secondary structure element	PaFtsZ	AaFtsZ	BsFtsZ	MtFtsZ	MjFtsZ	TmFtsZ
S1	I14	I6	I14	I11	I40	I24
	K15	K7	K15	K12	T41	K25
	V16	V8	V16	V13	V42	V26
	I17	I9	I17	V14	V43	I27
	G18	G10	G18	G15	G44	G28
	V19	V11	V19	I16	C45	V29
H1	G22	G14	G22	G19	A48	A32
	G23	G15	G23	G20	G49	G33
	G24	S16	N24	V21	N50	N34
	A26	A18	A26	A23	T52	A36
	V27	V19	V27	V24	I53	I37
	A31	Y23	I31	I28	K57	I41
S2	E39	E31	E39	E36	K65	E49
	F40	L32	Y40	F37	T66	F50
	I41	Y33	I41	I38	V67	V51
	C42	A34	A42	A39	A68	A52
	A43	I35	V43	I40	I69	V53
	N44	N36	N44	N41	N70	N54
S3	T57	N49	V57	V54	K83	V67
	Q60	Q52	Q60	D57	L86	Q70
S4	M98	M90	M98	M95	M124	M108
	V99	V91	V99	V96	V125	V109
	F100	F92	F100	F97	F126	F110
	I101	I93	V101	V98	I127	I111
	T102	S94	T102	T99	T128	T112
	T103	A95	A103	A100	C129	A113
	G104	G96	G104	G101	G130	G114
H4	G108	G100	G108	G105	G134	G118
	T109	T101	T109	T106	T135	T119
	G110	G102	G110	G107	G136	G120
	T111	T103	T111	T108	T137	T121
	G112	G104	G112	G109	G138	G122
	A113	A105	A113	G110	S139	A123
	A114	A106	A114	A111	A140	S124
	P115	P107	P115	P112	P141	P125
	I117	I109	I117	V114	V143	I127
	A118	A110	A118	A115	A144	A128
S5	L127	L119	L127	L124	L153	L137
	T128	T120	T128	T125	T154	T138
	V129	V121	V129	V126	V155	V139
	A130	A122	G130	G127	A156	A140
	V131	V123	V131	V128	V157	I141
	V132	A124	V132	V129	V158	V142
	T133	T125	T133	T130	T159	T143
	R134	L126	R134	R131	L160	T144
H5	R143	K135	R143	R140	R169	R153
	A147	A139	A147	A144	A173	A157
	G150	G142	G150	G147	G176	G160
	I151	L143	I151	I148	L177	L161
	L154	L146	M154	L151	L180	L164
S6	S160	A152	T160	T157	T186	T170
	L161	Y153	L161	L158	L187	L171
	I162	I154	I162	I159	V188	I172
	T163	V155	V163	V160	V189	K173
	I164	I156	I164	I161	I190	I174
	P165	H157	P165	P162	P191	S175

rmsd determination and inter-domain angle analysis					
PaFtsZ	AaFtsZ	BsFtsZ	MtFtsZ	MjFtsZ	TmFtsZ
M226	I218	M226	M223	I251	L238
C230	E222	I230	S227	E255	V242
T241	V233	A241	A238	V266	A253
N247	S238	S247	S244	S272	S259
I261	L253	V260	V257	A285	I272
T266	W258	T265	A262	M290	T277
Y276	V268	V275	I272	A300	V287
I283	I275	V282	V279	V307	I294
K294	I286	I293	I290	I318	K305
L307	I299	I306	V303	V331	I319
V313	I303	V310	V307	L335	F323

relevant. When performing pairwise alignments of structures it is possible to introduce bias towards the reference structure. Therefore, we first carried out the alignment using PaFtsZ as a reference and then generated averaged C^{α} positions of the 56 key residues from all the aligned structures (Figure 2; Table 2). Finally, the averaged C^{α} positions were used as the reference for alignment of all structures. Having aligned the FtsZ structures in this way, it is possible to detect subtle shifts in the relative positions of the N-terminal and C-terminal domains that would not be evident if the structures were aligned over the entire molecule.

Lack of conformational change between free and SulA-bound *P. aeruginosa* FtsZ

The previously determined structure of PaFtsZ in complex with SulA shows a SulA dimer bound to two FtsZ molecules.[41] SulA binds to and occludes the T7 loop surface of the FtsZ monomer, blocking the protofilament interface and preventing polymerization.[42] However, a recent analysis by Buey *et al.* found that superposition of MjFtsZ and PaFtsZ structures reveals a displacement of the H7 helix coupled with a movement of the C-terminal domain. Since this difference is reminiscent of the conformational changes thought to occur in the curved-to-straight conformational switch of tubulin, the authors concluded that MjFtsZ crystals show the monomer in its curved state while the PaFtsZ-SulA complex shows the monomer its a straight state. They further proposed that SulA binding, in addition to blocking the protofilament interface, might induce a conformational change that mimics the conformation of FtsZ in straight protofilaments. However, these conclusions remained tentative in the absence of structural data on SulA-free PaFtsZ.

A comparison of our new structure of SulA-free PaFtsZ with the previously published PaFtsZ-SulA complex shows no significant difference between the two (Figure 3), despite the different crystal contexts. Any change seen between the two structures is much smaller than those seen between FtsZ structures from different organisms (see below; Figure 4; Tables 3 and 4). Comparison of the structure of SulA-free PaFtsZ with the two PaFtsZ molecules in the asymmetric unit of the SulA-bound crystals shows that the differences between the SulA-free and SulA-bound structures are not greater than the differences between the two SulA-bound structures. The superposition of SulA-free FtsZ with SulA-bound molecule A shows that differences with chain A involve only small displacements of S2, loop T3, loop T7 (in the N-terminal domain), S9, S10 and loops in the protein surface (in the C-terminal domain) with an rmsd of 0.5 Å. Within molecule B, shifts are localized in H1, H2, loop H2-S3, H5, H6, H7 top, loop T7 (in the N-terminal domain), S9, S10 and loops on the protein surface (in the C-terminal domain) with a slightly bigger rmsd of 0.9 Å. The domain rotations of the C-terminal domain after alignment of the N-terminal domains of the free and

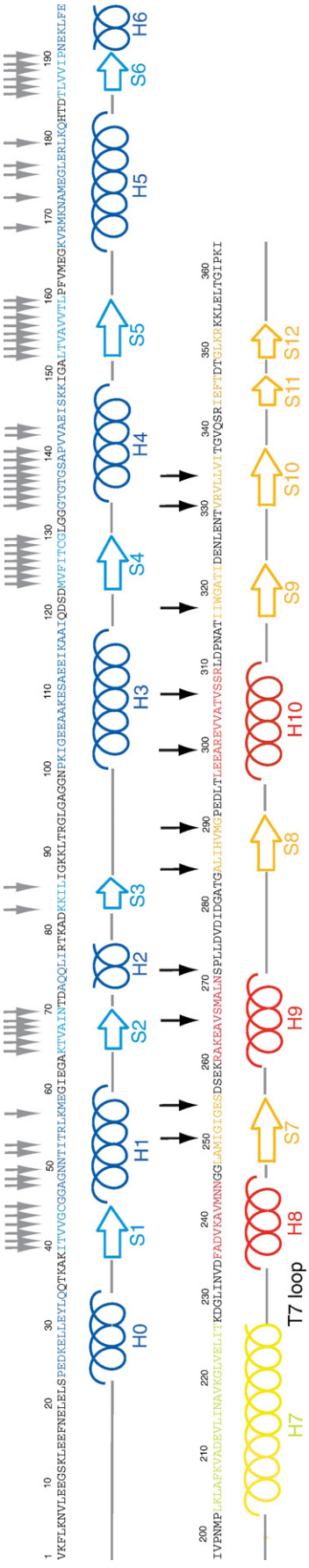

Figure 2. *M. jannaschii* FtsZ amino acid sequence and secondary structure. Secondary structure elements in the N-terminal domain are coloured dark/light blue, the central helix H7 is yellow and secondary structure elements in the C-terminal domain are in red/orange. Grey arrows in the nucleotide-binding domain indicate the core residues of the N-terminal domain chosen for structural alignments. Black arrows in the C-terminal domain indicate residues selected for calculating relative rmsd and rotation angles between the C-terminal domains.

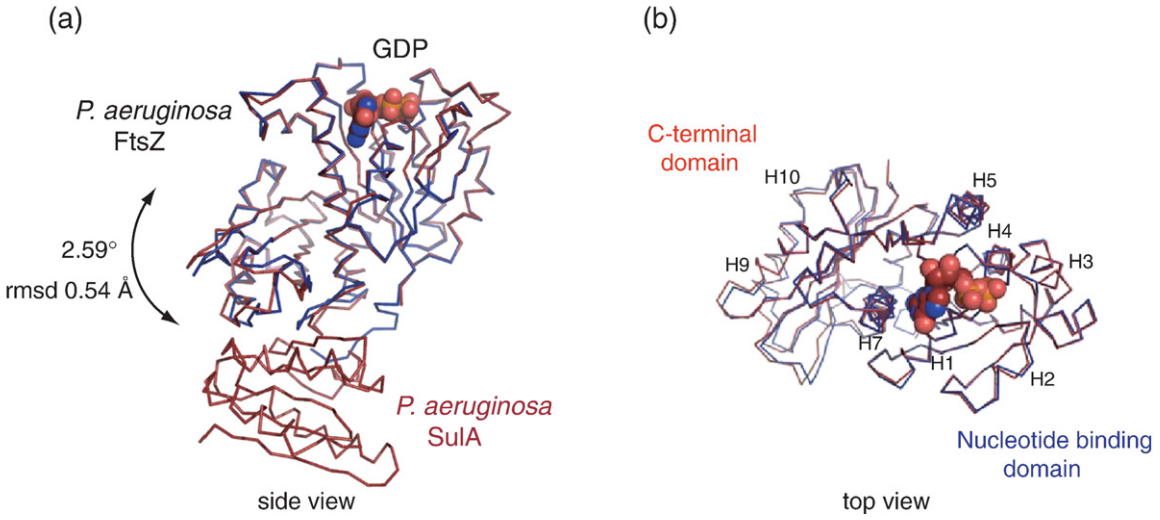

Figure 3. Ribbon representation of *P. aeruginosa* structure superposition in (a) side view and (b) top view. FtsZ in complex with the cell division inhibitor SulA is in dark-red (PDB ID 1OFU) and FtsZ without SulA (PDB ID 2VAW) is in blue. Both molecules have GDP in the nucleotide-binding pocket, shown in space-filling representation. FtsZ without SulA shows a 2.59° downward movement of the C-terminal domain. The lack of significant changes when comparing the free and SulA-bound form of FtsZ excludes a conformational change as proposed.[37]

SulA-bound structures are 2.59° (with chain A) and 2.09° (with chain B). Comparing the two molecules from the SulA-bound crystals, the largest changes involve H6, the top of H7 (in the N-terminal domain) and H9, H10, loop H9-S8 and loop S9-H10 (in the C-terminal domain) with an rmsd of 0.8 Å.

It appears that SulA inhibits FtsZ polymerisation simply by blocking the protofilament interface and preventing longitudinal association, rather than by inducing any substantial conformational change.

Absence of a nucleotide-dependent conformational change

It has been proposed that tubulin undergoes a nucleotide-dependent conformational change, and that this causes changes in the resulting polymer structures.[34] For FtsZ, we previously favoured a model that does not invoke such changes because no significant difference was observed between the crystal structures of MjFtsZ in the GDP and GTP states (PDB ID 1FSZ and 1W5E).[36] Analogous findings were reported in the case of γ-tubulin.[28]

Here, we use the improved structural alignment of all available structures of MjFtsZ in different nucleotide states (Table 3). GDP-bound (PDB ID 1FSZ) and GTP-bound mutant MjFtsZ (W319Y, PDB ID 1W5E) show an rmsd between their C-terminal domains of 1.0 Å and we consider this difference insignificant, taking the resolutions of the structures into account. Similarly, our new pair of AaFtsZ:GDP and AaFtsZ:8-morpholino-GTP show even smaller differences (rmsd 0.2 Å). We therefore conclude that there is no change of the inter-domain angle in the monomer caused by changes in the nucleotide state.

A slightly larger difference is seen between the GDP-bound state of the monomer of MjFtsZ (PDB ID 1FSZ) and the nucleotide-free form in the pseudo-protofilaments (PDB ID 1W59) involving an rmsd of 1.45 Å (Figure 4(a)), which implies a slight upward movement of the C-terminal domain, coupled with a sideways displacement of the top of helix H7. The differences between these two structures could be due to the nucleotide content or to the protofilament-like crystal packing, or both. Since the two different crystal forms of MjFtsZ-GDP have an rmsd for the C-terminal domain of 1.2 Å, we would consider that the differences shown in Figure 4(a) represent only the inherent flexibility of the FtsZ monomer rather than a nucleotide-dependent change.

Soaking experiments with different nucleotides also revealed no conformational change on FtsZ, as expected, since the crystal lattice imposes strong constraints. For example, a GMPCPP soak of previously GDP-containing MjFtsZ crystals shows an rmsd of only 0.4 Å (PDB IDs 1W58, 1FSZ).

Domain arrangements in other FtsZs

A comprehensive analysis of the superimposed structures of FtsZ from different organisms and in different states reveals that the most striking pairwise differences are seen in the comparisons between PaFtsZ and MjFtsZ, with a C^{α} rmsd of 2.67 Å calculated over the C-terminal domain (larger than the 1.84 Å rmsd reported for the previous analysis,[37] as these used a slightly different set of residues to align the N-terminal domain), PaFtsZ and BsFtsZ with a C^{α} rmsd of 2.46 Å, and AaFtsZ and BsFtsZ with an rmsd of 1.90 Å (Table 3; Figure 4(b)). These deviations are induced by a general downward movement of the PaFtsZ C-terminal domain followed by a sideways displacement of the top of H7 helix (Figure 4(a)). The rotation angle of the C-terminal domain shows the same trend as the C^{α}

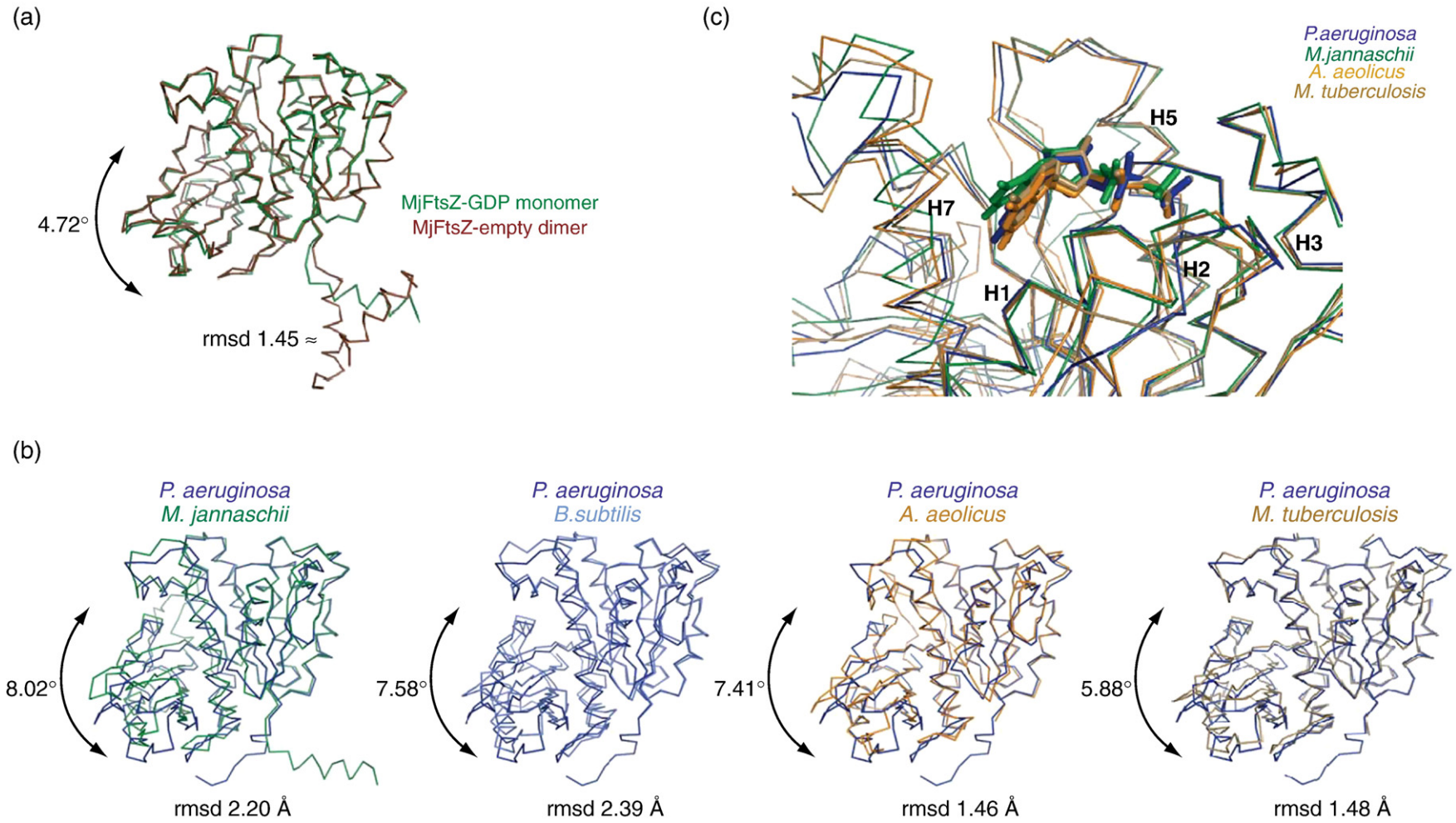

Figure 4. FtsZ structural superpositions. (a) Pairwise superposition of GDP-MjFtsZ (PDB ID 1FSZ) in dark green and empty MjFtsZ (PDB ID 1W59 chain A) in red showing the biggest structural differences when comparing two FtsZ structures from the same organism (rmsd 1.45 Å, 4.72° rotation). (b) Pairwise comparison of GDP-PaFtsZ without SulA (PDB ID 2VAW) in dark blue with GDP-MjFtsZ (PDB entry 1FSZ) in dark green (left), empty BsFtsZ (PDB ID 2VAM) in light blue (second from left), GDP-AaFtsZ (PDB ID 2RGR) in orange (third from left) and GDP-MtFtsZ (PDB ID 1RQ7 chain A) in brown (right). After aligning the nucleotide-binding domains, the C-terminal domains show upward movements from 1.46 Å to 2.39 Å. The same trend is reflected when calculating single rotation angles that vary between 5.88° to 8.02° between different FtsZ molecules. (c) GDP-bound PaFtsZ, MjFtsZ, AaFtsZ and MtFtsZ superposition showing the nucleotide-binding pocket. The guanine base of GDP points at a conserved Asp residue in helix H7 (Asp187, Asp212, Asp179 and Asp184, respectively). No large change can be seen, but the position of the base moves slightly due to the different position of H7 and the aspartic acid residues.

Table 3. rmsd values of key residues in the C-terminal domain after alignment of the N-terminal domains (in Å)

Methanococcus jannaschii																	
1W58	1W59-A	1W59-B	1W5B-A	1W5B-B	1W5A-A	1W5A-B	1W5E-A	1W5E-B	1W5E-C	1W5E-D	1W5E-E	1W5E-F	1W5E-G	1W5E-H	1W5E-I	2VAP-A	PDB entry
0.393	1.45	1.469	0.995	0.997	0.964	0.971	1.058	1.060	1.040	1.065	1.088	1.047	1.053	1.062	1.050	1.209	1FSZ
–	1.578	1.604	1.074	1.079	1.034	1.046	1.193	1.188	1.166	1.195	1.211	1.167	1.188	1.190	1.171	1.240	1W58
	–	0.118	0.591	0.561	0.620	0.598	0.551	0.555	0.601	0.540	0.523	0.577	0.554	0.552	0.585	0.609	1W59
		–	0.637	0.596	0.655	0.631	0.587	0.593	0.636	0.573	0.555	0.609	0.589	0.585	0.619	0.646	1W59
			–	0.207	0.139	0.194	0.409	0.402	0.422	0.399	0.398	0.393	0.401	0.403	0.406	0.405	1W5B
				–	0.227	0.169	0.388	0.397	0.432	0.387	0.403	0.421	0.382	0.396	0.421	0.360	1W5B
					–	0.088	0.417	0.421	0.432	0.401	0.404	0.403	0.411	0.411	0.415	0.379	1W5A
						–	0.394	0.393	0.421	0.378	0.385	0.395	0.389	0.392	0.404	0.358	1W5A
							–	0.089	0.165	0.073	0.126	0.163	0.053	0.098	0.159	0.523	1W5E
								–	0.112	0.109	0.097	0.113	0.096	0.052	0.108	0.513	1W5E
									–	0.183	0.166	0.09	0.165	0.119	0.058	0.558	1W5E
										–	0.090	0.154	0.084	0.105	0.166	0.504	1W5E
											–	0.115	0.134	0.090	0.144	0.492	1W5E
												–	0.160	0.104	0.065	0.527	1W5E
													–	0.086	0.150	0.513	1W5E
														–	0.095	0.505	1W5E
															–	0.532	1W5E

Pseudomonas aeruginosa			*Mycobacterium tuberculosis*			*Aquifex aeolicus*	*Bacillus subtilis*		
1OFU-A	1OFU-B	2VAW-A	1RQ2-A	1RQ7-A	1RLU-A	2RGR-A	2VAM-A	PDB entry	
2.151	2.784	2.202	1.607	1.782	1.759	1.453	2.149	1FSZ	*Methanococcus jannaschii*
2.065	2.687	2.117	1.612	1.778	1.761	1.365	2.212	1W58	
2.751	3.316	2.875	1.787	1.958	1.886	1.946	1.409	1W59-A	
2.774	3.342	2.896	1.815	1.983	1.911	1.988	1.425	1W59-B	
2.467	3.064	2.582	1.574	1.775	1.715	1.659	1.568	1W5B-A	
2.316	2.910	2.428	1.437	1.620	1.557	1.538	1.410	1W5B-B	
2.408	3.012	2.521	1.537	1.733	1.673	1.620	1.551	1W5A-A	
2.374	2.977	2.489	1.508	1.699	1.638	1.594	1.506	1W5A-B	
2.428	3.009	2.537	1.614	1.797	1.737	1.627	1.514	1W5E-A	
2.436	3.019	2.584	1.606	1.792	1.731	1.630	1.511	1W5E-B	
2.420	2.998	2.566	1.613	1.800	1.741	1.614	1.542	1W5E-C	
2.449	3.032	2.595	1.637	1.820	1.759	1.644	1.528	1W5E-D	
2.483	3.069	2.634	1.650	1.835	1.774	1.674	1.533	1W5E-E	
2.455	3.042	2.604	1.634	1.822	1.763	1.647	1.559	1W5E-F	
2.417	3.000	2.561	1.593	1.777	1.717	1.615	1.498	1W5E-G	
2.434	3.019	2.582	1.601	1.786	1.726	1.627	1.505	1W5E-H	
2.431	3.012	2.578	1.612	1.799	1.740	1.619	1.535	1W5E-I	
2.389	2.983	2.528	1.462	1.650	1.586	1.618	1.328	1JZ17-A	
–	0.818	0.541	1.492	1.413	1.433	1.341	2.272	1OFU-A	*Pseudomonas aeruginosa*
	–	0.894	2.106	1.986	2.018	1.760	2.735	1OFU-B	
		–	1.580	1.477	1.509	1.455	2.393	2VAW-A	
			–	0.259	0.229	1.335	1.218	1RQ2-A	*Mycobacterium tuberculosis*
				–	0.130	1.376	1.262	1RQ7-A	
					–	1.382	1.189	1RLU-A	
						–	1.901	2RGR-A	*Aquifex aeolicus*

Table 4. Angles between C-terminal domains after alignment of the N-terminal domains of FtsZ

Organism	PDB entry	Rotation angle (deg.)
Methanococcus jannaschii	1FSZ	8.02
	1W58	8.26
	1W59-A	8.24
	1W59-B	7.88
	1W5B-A	8.81
	1W5B-B	7.52
	1W5A-A	8.33
	1W5A-B	7.99
	1W5E-A	8.77
	1W5E-B	8.81
	1W5E-C	8.99
	1W5E-D	8.82
	1W5E-E	8.89
	1W5E-F	9.02
	1W5E-G	8.71
	1W5E-H	8.77
	1W5E-I	8.99
	2VAP	8.04
Pseudomonas aeruginosa	1OFU-A	2.59
	1OFU-B	2.09
Mycobacterium tuberculosis	1RQ2-A	5.77
	1RQ7-A	5.88
	1RLU-A	5.74
Aquifex aeolicus	2RGR	7.41
Bacillus subtilis	2VAM	7.58

After aligning against the averaged reference, angles were calculated relative to PaFtsZ (PDB ID 2VAW).

rmsd measurements (Table 4): the biggest difference in angle is observed between PaFtsZ and MjFtsZ (8.02°); the rotation angles of the PaFtsZ C-terminal domain relative to BsFtsZ, AaFtsZ and MtFtsZ are 7.6°, 7.4° and 5.8°, respectively. The differences in the position of helix H7 relative to the N-terminal domain can be seen clearly by examining the position of the nucleotide in the different structures (Figure 4(c)), where the guanosine forms a hydrogen bond with a conserved Asp residue in helix H7, and differences in the position of this helix relative to the N-terminal domain lead to slightly different orientations of the nucleotide.

PaFtsZ and MjFtsZ show the biggest differences in C-terminal domain position, while BsFtsZ, MtFtsZ and AaFtsZ display an intermediate position between the two extremes. BsFtsZ is closer to MjFtsZ with an rmsd of 1.63 Å. AaFtsZ and MtFtsZ have a C-terminal domain position roughly intermediate between PaFtsZ and MjFtsZ, with rmsd values of 1.51 Å and 1.64 Å (AaFtsZ), and 1.7 Å and 1.63 Å (MtFtsZ). These rmsd values are an average of all those from FtsZ structures of a single organism when it is applicable (Table 3). This comparison shows clear evidence of structural differences among FtsZ homologues from different organisms. These differences do not appear to correlate with phylogenetic groupings, crystallization conditions or truncations of the construct used for crystallization, and probably represent no more than the natural differences between structures that would be expected on the basis of their different primary sequences. Sequence alignments of these FtsZ homologues shows an identity of 33–54%, of which most similarity is located in the N-terminal domain.

Lattice versus strain model

The structural data and analysis presented here suggest a revised model of the straight-to-curved transition in the protofilament (Figure 5). Although it is possible that future structural data on FtsZ may reveal a nucleotide-induced conformational change in the monomer, we consider this highly unlikely, given the fact that we have analysed a large number of structures from several different species, in

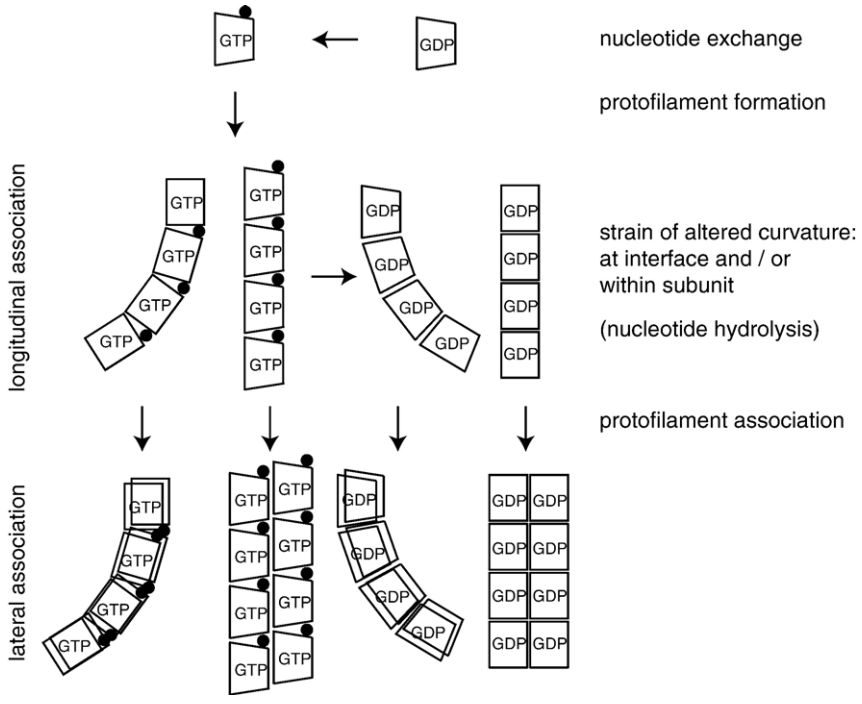

Figure 5. The Lattice *versus* Strain model. The central idea is that lateral interactions can stabilise a strained conformation of the protofilament. The monomer shows no change in conformation related to the nucleotide state. Single protofilaments may prefer to adopt straight or curved conformations, depending on the nucleotide state. Increasing or decreasing the curvature introduces some degree of strain, which may result in distortion of the protofilament interface or the monomer conformation. In higher-order structures formed by lateral association of single protofilaments, the strain of curvature can be offset by the energy of the lateral interactions.

different nucleotide states (GTP, GDP and empty), and in the presence and in the absence of bound inhibitory proteins, and found no evidence of such a conformational change. In the tubulin field, this relates to similar data obtained with γ-tubulin.[28]

Central to our proposal is the observation that FtsZ monomers (and probably tubulin as well) and the protofilament interfaces have a flexibility that allows the molecules to balance different sources and sinks of energy in the system. Starting with the GDP form of the monomer, the immediate effect of GDP to GTP exchange is to promote longitudinal association of monomers into protofilaments; no conformational change in the monomer takes place at this stage. Once formed, the protofilaments will have some flexibility and can adopt different curvatures by bending at the interfaces between subunits and perhaps within the subunits themselves.[26,43] In higher-order structures formed by lateral association of single protofilaments, the strain of curvature can be offset by the energy of the lateral interactions. The currently accepted view of protofilament structure is that the GDP-bound form of the protofilament is intrinsically curved, while the GTP-bound form is straight. However, the majority of experimental data on filaments of both FtsZ and tubulin have been obtained in the presence of interactions that may alter the filament curvature: crystal packing, bundling of filaments or adsorption onto electron microscope grids. We believe that current proposals for the structure of the single protofilament remain speculative.

High-resolution structural information is missing for two crucial states of our model. For FtsZ, there is currently no structural model of the protofilament in a state that has appropriate lateral interactions. An experimentally determined structure of FtsZ in laterally associated filaments could reveal details of changes at the protofilament interface and perhaps also within the monomer. These changes might include a shift in the angle between the N-terminal and C-terminal domains similar to that observed for tubulin.

Similarly, we expect that a high-resolution structure of αβ-tubulin in the absence of lateral interactions would reveal the free conformation of the tubulin dimer. This would allow us to decide whether the tubulin dimer is intrinsically curved in the absence of additional sources of energy (stathmin binding or lateral interactions) and whether this conformation indeed involves changes in the angle between the N-terminal and C-terminal domains. Unfortunately, the structures of FtsZ in straight protofilaments and free tubulin are not available.

Materials and Methods

Protein expression and purification

FtsZ from *M. jannaschii* was expressed and purified as described.[36]

FtsZ from *P. aeruginosa* (1-318) was cloned as described.[41] The protein was purified as described (method 1, precipitation in ammonium sulfate) with minor modifications.[44] After precipitation in 30% ammonium sulfate saturation and anion-exchange chromatography, the protein was dialyzed against 50 mM Tris–HCl (pH 8.0), 200 mM KCl, 1 mM EDTA, 10% (v/v) glycerol and subjected to gel-filtration chromatography in the same buffer using a Sephacryl S200 26/60 column (Amersham). The purest fractions were concentrated to 10 g/l and used directly for crystallization. The nucleotide content was measured as described.[20]

Untagged, full-length *ftsZ* from *B. subtilis* (ATCC 23857D) was cloned into NdeI and BamHI of pHis17. Sequencing of multiple independent clones revealed three modifications relative to the published database sequence: *cgc* to *cgt* (a silent mutation in the codon for R332), *gac* to *gag* (D350E) and *gca* to *cca* (A351P). These changes were assumed to be due to strain differences or errors in the database sequence. The protein was purified by precipitation in 30% ammonium sulfate in 50 mM Tris–HCl (pH 8.0), 50 mM KCl, 1 mM EDTA, 10 mM $MgCl_2$, followed by anion-exchange chromatography with a 5 ml HiTrap Q HP column (Amersham) in 50 mM Mes–KOH (pH 6.5), 5 mM $MgCl_2$ where FtsZ was eluted with 300 mM KCl. Finally the protein was subjected to gel-filtration chromatography (Sephacryl S300 26/60 column, Amersham) in 50 mM Tris–HCl (pH 7.5), 1 mM EDTA, 1 mM NaN_3, concentrated to 15 g/l and stored at −80 °C.

C-terminally truncated *A. aeolicus* FtsZ (residues 1–330) was cloned into NdeI and HindIII of pHis17, yielding a C-terminally His_6-tagged fusion protein. The protein was expressed in *Escherichia coli* BL21-AI cells (Invitrogen). Exponential growth phase cells ($A_{600}=0.7$) were induced for 4 h by the addition of 0.3% (w/v, final concentration) arabinose. The protein was purified by HisTrap nickel-affinity chromatography followed by gel-filtration chromatography on a Sephacryl S200 column in 20 mM Tris–HCl (pH 7.5), 1 mM EDTA and 1 mM NaN_3. Fractions containing highly pure FtsZ were concentrated to 15 g/l and stored at −80 °C.

Crystallization and structure determination

All crystals were grown at 19 °C using the sitting-drop. vapour-diffusion technique and initial hits were found using our in-house nanolitre crystallization facility.[45] Diffraction data was collected at the ESRF (Grenoble, France). Data were integrated and reduced using MOSFLM and SCALA.[46] Structure solution and refinement were performed using CNS[47] or REFMAC.[48]

MjFtsZ (PDB ID 2VAP) crystals were grown over a reservoir solution containing 0.1 M Bis-Tris propane (pH 7.0) and 4.0 M ammonium acetate. Drops were composed of 100 nl of protein at 10.0 g/l (with 8 mM $MgCl_2$, 8 mM NaF, 200 μM $AlCl_3$, 1 mM GDP) and 100 nl of reservoir solution (AlF_3 was not visible in the electron density). Crystals were cryoprotected with 25% (v/v) glycerol. The structure was solved by molecular replacement with 1FSZ as the model.

PaFtsZ crystals were grown over a reservoir solution containing 0.1 M Bis-Tris (pH 5.8), 26% (w/v) PEG2000-MME. Drops were composed of 200 nl of protein (10.0 g/l) and 200 nl of reservoir solution. The cryobuffer was crystallization solution plus 15% (w/v) PEG200. Molecular replacement was carried out using the PaFtsZ monomer from PDB ID 1OFU as the search model.

BsFtsZ crystals were grown over a reservoir solution containing 0.1 M Mes–NaOH (pH 6.0), 0.24 M $(NH_4)_2SO_4$, 11% (w/v) PEG8000 and drops were composed of 500 nl of protein solution (containing 0.5 mM protein and 3 mM dichamanetin from a 100 mM stock solution in DMSO) plus 500 nl of reservoir. Dichamanetin inhibits the GTPase

activity of FtsZ,[38] and was obtained from the authors. Before flash-cooling, the crystals were placed in mother liquor plus 15% glycerol. Molecular replacement was carried out using the PaFtsZ monomer as a search model (PDB ID 1OFU).

AaFtsZ crystals were grown by adding 2 mM $MgCl_2$ and 1 mM GDP (final concentrations) to the protein sample (15 g/l) and crystallizing over a reservoir solution containing 0.1 M Mops–NaOH (pH 6.5), 0.2 M NaCl, 28% (w/v) PEG400. Drops were composed of 500 nl of protein solution and 500 nl of reservoir solution. No additional cryoprotectant was added to the crystals before flash freezing. Diffraction data were collected to 1.7 Å on a Rigaku RU-300 rotating anode. Molecular replacement was performed with MjFtsZ (PDB ID 1FSZ) as the search model.

Alignment of FtsZ structures

To select the core secondary structure residues of the N-terminal domain, we performed an initial multiple structural alignment of FtsZ homologues from *P. aeruginosa*, *A. aeolicus*, *B. subtilis*, *M. tuberculosis*, *M. jannaschii* and *T. maritima* FtsZ using the MSDFold web server.[49] We selected 56 core residues that are located within secondary structure elements of the N-terminal domain of FtsZ, choosing the residues that were less than 2 Å apart in the alignment and were located in the interior of the protein, thus excluding regions of the structure that might be distorted by crystal contacts (see Figure 2, grey arrows). All structures were aligned on the basis of these core residues against PaFtsZ (PDB ID 1OFU) and superimposed. We then calculated the average C^{α} coordinates for the 56 residues of the N-terminal domain core (one structure per organism only) and used these as a new reference PDB file for all structures, including PaFtsZ in a second round of alignment.

The rmsd values of the C-terminal domains after aligning the N-terminal domains were calculated using 11 selected residues located on core secondary structural elements of that domain (see Figure 2, black arrows). Rotation angles were calculated using the same residues.

Acknowledgements

We are grateful to Dr Jared Shaw (Harvard, Cambridge, MA) for providing us with Dichamnetin. We thank EMBO for supporting M.A.O. with a long-term fellowship (ALF-1712005). D.T. was supported by an LMB Cambridge Student Scholarship. Diffraction data were collected at beamlines ID29, ID23 and ID14 at the ESRF (Grenoble, France), and we thank the beamline staff for excellent support.

References

1. Bi, E. F. & Lutkenhaus, J. (1991). FtsZ ring structure associated with division in Escherichia coli. *Nature*, **354**, 161–164.
2. Stricker, J., Maddox, P., Salmon, E. D. & Erickson, H. P. (2002). Rapid assembly dynamics of the *Escherichia coli* FtsZ-ring demonstrated by fluorescence recovery after photobleaching. *Proc. Natl Acad. Sci. USA*, **99**, 3171–3175.
3. Mukherjee, A., Dai, K. & Lutkenhaus, J. (1993). *Escherichia coli* cell division protein FtsZ is a guanine nucleotide binding protein. *Proc. Natl Acad. Sci. USA*, **90**, 1053–1057.
4. Bramhill, D. & Thompson, C. M. (1994). GTP-dependent polymerization of *Escherichia coli* FtsZ protein to form tubules. *Proc. Natl Acad. Sci. USA*, **91**, 5813–5817.
5. Romberg, L. & Levin, P. A. (2003). Assembly dynamics of the bacterial cell division protein FTSZ: poised at the edge of stability. *Annu. Rev. Microbiol.* **57**, 125–154.
6. Errington, J., Daniel, R. A. & Scheffers, D. J. (2003). Cytokinesis in bacteria. *Microbiol. Mol. Biol. Rev.* **67**, 52–65.
7. Weiss, D. S. (2004). Bacterial cell division and the septal ring. *Mol. Microbiol.* **54**, 588–597.
8. Michie, K. A. & Löwe, J. (2006). Dynamic filaments of the bacterial cytoskeleton. *Annu. Rev. Biochem.* **75**, 467–492.
9. Graumann, P. L. (2006). Cytoskeletal elements in bacteria. *Annu. Rev. Microbiol*, doi:10.1146/annurev.micro.61.080706.093236.
10. Varma, A. & Young, K. D. (2004). FtsZ collaborates with penicillin binding proteins to generate bacterial cell shape in *Escherichia coli*. *J. Bacteriol.* **186**, 6768–6774.
11. Aaron, M., Charbon, G., Lam, H., Schwarz, H., Vollmer, W. & Jacobs-Wagner, C. (2007). The tubulin homologue FtsZ contributes to cell elongation by guiding cell wall precursor synthesis in Caulobacter crescentus. *Mol. Microbiol.* **64**, 938–952.
12. Varma, A., de Pedro, M. & Young, K. D. (2007). FtsZ directs a second mode of peptidoglycan synthesis in *Escherichia coli*. *J. Bacteriol.* **15**, 5692–5704.
13. Löwe, J. & Amos, L. A. (1998). Crystal structure of the bacterial cell-division protein FtsZ. *Nature*, **391**, 203–206.
14. Nogales, E., Wolf, S. G. & Downing, K. H. (1998). Structure of the alpha beta tubulin dimer by electron crystallography. *Nature*, **391**, 199–203.
15. Nogales, E., Downing, K. H., Amos, L. A. & Löwe, J. (1998). Tubulin and FtsZ form a distinct family of GTPases. *Nature, Struct. Biol.* **5**, 451–458.
16. Desai, A. & Mitchison, T. J. (1997). Microtubule polymerization dynamics. *Annu. Rev. Cell Dev. Biol.* **13**, 83–117.
17. Molodtsov, M. I., Grishchuk, E. L., Efremov, A. K., McIntosh, J. R. & Ataullakhanov, F. I. (2005). Force production by depolymerizing microtubules: a theoretical study. *Proc. Natl Acad. Sci. USA*, **102**, 4353–4358.
18. Westermann, S., Wang, H. W., Avila-Sakar, A., Drubin, D. G., Nogales, E. & Barnes, G. (2006). The Dam1 kinetochore ring complex moves processively on depolymerizing microtubule ends. *Nature*, **440**, 565–569.
19. Gonzalez, J. M., Jimenez, M., Velez, M., Mingorance, J., Andreu, J. M., Vicente, M. & Rivas, G. (2003). Essential cell division protein FtsZ assembles into one monomer-thick ribbons under conditions resembling the crowded intracellular environment. *J. Biol. Chem.* **278**, 37664–37671.
20. Oliva, M. A., Huecas, S., Palacios, J. M., Martin-Benito, J., Valpuesta, J. M. & Andreu, J. M. (2003). Assembly of archaeal cell division protein FtsZ and a GTPase-inactive mutant into double-stranded filaments. *J. Biol. Chem.* **278**, 33562–33570.
21. Lu, C., Reedy, M. & Erickson, H. P. (2000). Straight and

curved conformations of FtsZ are regulated by GTP hydrolysis. *J. Bacteriol.* **182**, 164–170.
22. Huecas, S. & Andreu, J. M. (2004). Polymerization of nucleotide-free, GDP- and GTP-bound cell division protein FtsZ: GDP makes the difference. *FEBS Letters*, **569**, 43–48.
23. Mingorance, J., Rueda, S., Gomez-Puertas, P., Valencia, A. & Vicente, M. (2001). *Escherichia coli* FtsZ polymers contain mostly GTP and have a high nucleotide turnover. *Mol. Microbiol.* **41**, 83–91.
24. Chen, Y. & Erickson, H. P. (2005). Rapid in vitro assembly dynamics and subunit turnover of FtsZ demonstrated by fluorescence resonance energy transfer. *J. Biol. Chem.* **280**, 22549–22554.
25. Li, H., DeRosier, D. J., Nicholson, W. V., Nogales, E. & Downing, K. H. (2002). Microtubule structure at 8 Å resolution. *Structure*, **10**, 1317–1328.
26. Ravelli, R. B., Gigant, B., Curmi, P. A., Jourdain, I., Lachkar, S., Sobel, A. & Knossow, M. (2004). Insight into tubulin regulation from a complex with colchicine and a stathmin-like domain. *Nature*, **428**, 198–202.
27. Wang, H. W. & Nogales, E. (2005). Nucleotide-dependent bending flexibility of tubulin regulates microtubule assembly. *Nature*, **435**, 911–915.
28. Aldaz, H., Rice, L. M., Stearns, T. & Agard, D. A. (2005). Insights into microtubule nucleation from the crystal structure of human gamma-tubulin. *Nature*, **435**, 523–527.
29. Schlieper, D., Oliva, M. A., Andreu, J. M. & Löwe, J. (2005). Structure of bacterial tubulin BtubA/B: evidence for horizontal gene transfer. *Proc. Natl Acad. Sci. USA*, **102**, 9170–9175.
30. Schlichting, I., Almo, S. C., Rapp, G., Wilson, K., Petratos, K., Lentfer, A. *et al.* (1990). Time-resolved X-ray crystallographic study of the conformational change in Ha-Ras p21 protein on GTP hydrolysis. *Nature*, **345**, 309–315.
31. Wittinghofer, A. & Pai, E. F. (1991). The structure of Ras protein: a model for a universal molecular switch. *Trends Biochem. Sci.* **16**, 382–387.
32. Kjeldgaard, M., Nissen, P., Thirup, S. & Nyborg, J. (1993). The crystal structure of elongation factor EF-Tu from *Thermus aquaticus* in the GTP conformation. *Structure*, **1**, 35–50.
33. Roll-Mecak, A., Cao, C., Dever, T. E. & Burley, S. K. (2000). X-ray structures of the universal translation initiation factor IF2/eIF5B: conformational changes on GDP and GTP binding. *Cell*, **103**, 781–792.
34. Nogales, E. & Wang, H. W. (2006). Structural mechanisms underlying nucleotide-dependent self-assembly of tubulin and its relatives. *Curr. Opin. Struct. Biol.* **16**, 221–229.
35. Nogales, E. & Wang, H. W. (2006). Structural intermediates in microtubule assembly and disassembly: how and why? *Curr. Opin. Cell Biol.* **18**, 179–184.
36. Oliva, M. A., Cordell, S. C. & Löwe, J. (2004). Structural insights into FtsZ protofilament formation. *Nature Struct. Mol. Biol.* **11**, 1243–12450.
37. Buey, R. M., Diaz, J. F. & Andreu, J. M. (2006). The nucleotide switch of tubulin and microtubule assembly: a polymerization-driven structural change. *Biochemistry*, **45**, 5933–5938.
38. Urgaonkar, S., La Pierre, H. S., Meir, I., Lund, H., RayChaudhuri, D. & Shaw, J. T. (2005). Synthesis of antimicrobial natural products targeting FtsZ: (+/-)-dichamanetin and (+/-)-2′ ″-hydroxy-5′ ′-benzylisouvarinol-B. *Org. Letters*, **7**, 5609–5612.
39. Erickson, H. P., Taylor, D. W., Taylor, K. A. & Bramhill, D. (1996). Bacterial cell division protein FtsZ assembles into protofilament sheets and minirings, structural homologs of tubulin polymers. *Proc. Natl Acad. Sci. USA*, **93**, 519–523.
40. Wang, H. W., Long, S., Finley, K. R. & Nogales, E. (2005). Assembly of GMPCPP-bound tubulin into helical ribbons and tubes and effect of colchicine. *Cell Cycle*, **4**, 1157–1160.
41. Cordell, S. C., Robinson, E. J. & Lowe, J. (2003). Crystal structure of the SOS cell division inhibitor SulA and in complex with FtsZ. *Proc. Natl Acad. Sci. USA*, **100**, 7889–7894.
42. Mukherjee, A., Cao, C. N. & Lutkenhaus, J. (1998). Inhibition of FtsZ polymerization by SulA, an inhibitor of septation in *Escherichia coli*. *Proc. Natl Acad. Sci. USA*, **95**, 2885–2890.
43. Nicholson, W. V., Lee, M., Downing, K. H. & Nogales, E. (1999). Cryo-electron microscopy of GDP-tubulin rings. *Cell Biochem. Biophys.* **31**, 175–183.
44. Rivas, G., Lopez, A., Mingorance, J., Ferrandiz, M. J., Zorrilla, S., Minton, A. P. *et al.* (2000). Magnesium-induced linear self-association of the FtsZ bacterial cell division protein monomer. The primary steps for FtsZ assembly. *J. Biol. Chem.* **275**, 11740–11749.
45. Stock, D., Perisic, O. & Löwe, J. (2005). Robotic nanolitre protein crystallisation at the MRC Laboratory of Molecular Biology. *Prog. Biophys. Mol. Biol.* **88**, 311–327.
46. Collaborative Computational Project Number 4. (1994). The CCP4 suite: programs for protein crystallography. *Acta Crystallog. sect. D*, **50**, 760–763.
47. Brunger, A. T., Adams, P. D., Clore, G. M., DeLano, W. L., Gros, P., Grosse-Kunstleve, R. W. *et al.* (1998). Crystallography & NMR system: a new software suite for macromolecular structure determination. *Acta Crystallog. sect. D*, **54**, 905–921.
48. Murshudov, G. N., Vagin, A. A. & Dodson, E. J. (1997). Refinement of macromolecular structures by the maximum-likelihood method. *Acta Crystallog. sect. D*, **53**, 240–255.
49. Krissinel, E. & Henrick, K. (2004). Secondary-structure matching (SSM), a new tool for fast protein structure alignment in three dimensions. *Acta Crystallog. sect. D*, **60**, 2256–2268.